Plastic Moment of Intermediate Horizontal Boundary Elements of Steel Plate Shear Walls

BING QU and MICHEL BRUNEAU

ABSTRACT

This paper presents results of an analytical study of plastic moment in horizontal boundary elements (HBEs) in steel plate shear walls. To account for the effect of shear and vertical stresses in HBE web, the reduced axial yield strength was studied using the von Mises yield criterion. In the spirit of classic plastic analysis, analytical procedures for estimating plastic moment of the intermediate HBE under equal top and bottom tension fields are developed. Those analytical procedures are then extended for intermediate HBE under unequal top and bottom tension fields. Both positive and negative flexures are considered. Results from the analytical procedures are shown to agree well with those from finite element analysis. Simplified models for estimating plastic moment of HBEs are also developed for design and shown to be accurate.

Keywords: steel plate shear walls; horizontal boundary elements; plastic moments.

A special plate shear wall (SPSW) consists of unstiffened infill steel panels bounded by columns, called vertical boundary elements (VBEs), on both sides and beams, called horizontal boundary elements (HBEs), above and below. These panels are allowed to buckle in shear and subsequently form diagonal tension fields to resist lateral forces. Past experimental studies in the United States, Canada, Japan, Taiwan, and other countries have shown that SPSW can exhibit high initial stiffness, behave in a ductile manner and dissipate significant amounts of hysteretic energy—which make it a viable option for the design of new buildings as well as for the retrofit of existing constructions (an extensive literature review is available in Sabelli and Bruneau, 2006). Analytical research on SPSW has also validated useful models for the design and analysis of this system (e.g., Thorburn et al., 1983; Elgaaly et al., 1993; Driver et al., 1997; Berman and Bruneau, 2003b). Recent design procedures for SPSW are provided by the CSA *Limit States Design of Steel Structures* (CSA, 2009) and the AISC *Seismic Provisions for Structural Steel Buildings* (AISC, 2010). Innovative SPSW designs have also been proposed and experimentally validated to expand the range of applicability of SPSW (Berman and Bruneau, 2003a, 2003b; Vian and Bruneau, 2005).

Bing Qu, Assistant Professor, Department of Civil and Environmental Engineering, California Polytechnic State University, San Luis Obispo, CA (corresponding author). E-mail: bqu@calpoly.edu

Michel Bruneau, Professor, Department of Civil, Structural and Environmental Engineering, University at Buffalo, Buffalo, NY. E-mail: bruneau@buffalo.edu

However, this remains a relatively new structural system for seismic applications and is still the subject of much study. In particular, in an experimental study on full-scale two-story SPSWs conducted to investigate the seismic behavior of intermediate HBEs with reduced beam section (RBS) connections (Qu et al., 2008), the yield pattern of RBS in the intermediate HBE was different from expected. In conventional steel moment frames, plastic hinges are typically observed at the center of RBS. However, instead of forming at the RBS centers, the HBE plastic hinges moved toward the near column faces in the tested SPSW (i.e., developed in a zone between the RBS center and the HBE end). Likewise, similar yielding behavior of intermediate HBEs having RBS connections was consistently observed from recent experimental investigations on SPSWs (Tsai and Lee, 2007). These discrepancies in observed versus expected yielding behavior of intermediate HBE suggest that plastic moment in intermediate HBEs deserves to be further studied. Some detailed information about the aforementioned yield pattern of intermediate HBE was shown in Qu and Bruneau (2010).

Conventional simple plastic analysis procedures for determining the plastic moment of wide flange members in a steel moment frame cannot be applied to intermediate HBEs of SPSWs because the web of an HBE is under large biaxial stresses when the tension fields of the wall develop. To account for this effect—and consequently ensure predictable and ductile behavior of intermediate HBEs—analytical procedures to correctly quantify the strength of plastic hinges in HBEs subjected to axial force, shear force and vertical stresses due to infill panel forces are needed.

This paper first discusses the loading characteristics of HBE cross sections. Following a review of the classic plastic analysis procedure to calculate the plastic moment of wide flange members in steel moment frames, the reduced axial

yield strength of HBE web under shear and vertical stresses is studied using the von Mises yield criterion. Then, the analytical procedures for estimating the plastic moment of intermediate HBEs under equal and unequal top and bottom tension fields are respectively presented. Those procedures are verified by finite element (FE) examples and simplified for practical use. Finally, additional comments are given to anchor HBEs, defined in the next section. The procedures to estimate the plastic moment of intermediate HBE developed in this paper can be used in capacity design of intermediate HBEs (Qu and Bruneau, 2010).

LOADING CHARACTERISTICS OF HBE CROSS SECTIONS

In any multistory SPSW such as the one shown in Figure 1, HBEs can be classified as anchor HBEs and intermediate HBEs. Anchor HBEs are the top and bottom ends of a SPSW, and they anchor the infill panel yield forces. Because they are loaded by tension fields only on one side (either above or below), they are typically of substantial size. Intermediate HBEs are the beams at all levels other than the top and bottom of the SPSW. The variation between the top and bottom infill panel forces acting on intermediate HBE can sometimes be small (or nil) when the top and bottom infill panels of identical (or near identical) thicknesses are both yielding. Compared with the sizes of anchor HBEs, intermediate HBEs are often relatively small.

To understand the infill panel effects on HBE behavior, the aforementioned SPSW with rigid HBE-to-VBE connections is considered. The loading conditions at the ends of HBEs when the wall develops the expected plastic collapse mechanism are schematically shown in Figure 2. In this figure, τ represents the shear stress in HBE web; P and M represent the axial compression force and moment acting at HBE ends, respectively; and ω_{ybi+1} and ω_{ybi} represent the vertical components of the top and bottom infill tension fields, respectively. Mathematical expressions for ω_{ybi+1} and ω_{ybi} are given in Qu and Bruneau (2010).

Note that an HBE is typically in compression when the expected plastic mechanism of the SPSW develops as described in Qu and Bruneau (2010). The magnitudes of τ, P, and M may vary at different locations along the HBE. Although the direction of shear stress, τ, depends on the resulting shear effects due to infill tension fields and HBE flexural actions, it has no impact on HBE plastic moment as demonstrated later. Accordingly, the loading characteristics of HBE cross-sections are summarized in Table 1. Note that for the purpose of the present discussion, flexure designated as plus (+) or minus (–) respectively refers to the bending action producing tension or compression in the flange on which the greater tension field is applied. For intermediate HBEs under equal top and bottom tension fields, the acting direction of flexure has no impact on the plastic moment resistance as shown later.

PLASTIC MOMENT OF WIDE FLANGE IN MEMBER MOMENT FRAME

A well-known lower bound approach to estimate the plastic moment of wide flange member in steel moment frame, based on stress diagrams, and classic plastic analysis can be used to account for the combined interaction of flexure, axial force, and shear force (Bruneau et al. 1998). Using this procedure, the uniform shear stress, τ_w, assumed to act on

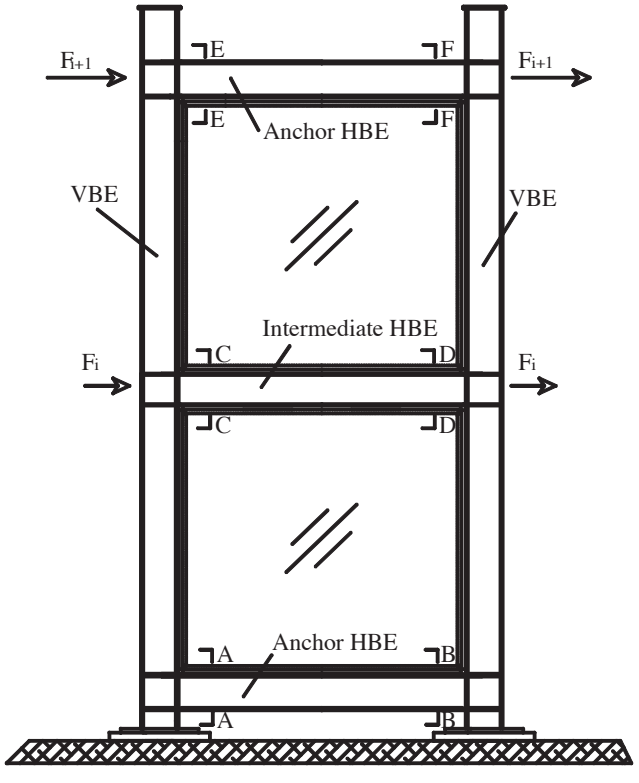

Fig. 1. A typical multistory SPSW.

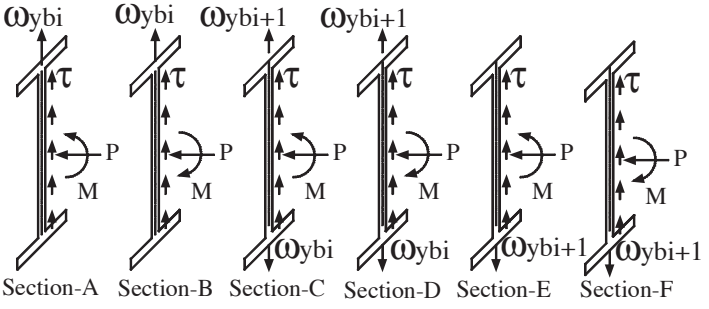

Fig. 2. Loading at HBE ends.

Table 1. Loading Characteristics of HBE Cross Sections				
HBE type	Corresponding Cross Section for Figure 1	Flexure		Ratio of Tension Fields $\omega_{yi}/\omega_{yi+1}$
		+	–	
Intermediate	C/D			1
Intermediate	C	✓		>1
Intermediate	D		✓	>1
Anchor	A		✓	0*
Anchor	B	✓		0*
Anchor	E	✓		∞**
Anchor	F		✓	∞**
*when $\omega_{yi} = 0$. ** when $\omega_{yi}+1 = 0$.				

the web of the section as a result of the applied shear force, *V*, is calculated as:

$$\tau_w = \frac{V}{h_w t_w} \tag{1}$$

where h_w and t_w are depth and thickness of the web of the cross section, respectively.

Then, the von Mises yield criterion is used to calculate the maximum axial stress, σ_w, that can be applied on the web (i.e., the remaining axial yield strength):

$$\sigma_w = \sqrt{f_y^2 - 3\tau_w^2} \tag{2}$$

where f_y is the yield strength of steel.

The strength of the flanges remains f_y. In the case where the neutral axis remains in the web, as shown in Figure 3, location of the neutral axis, y_0, is given by:

$$y_o = \frac{P}{2\sigma_w t_w} \tag{3}$$

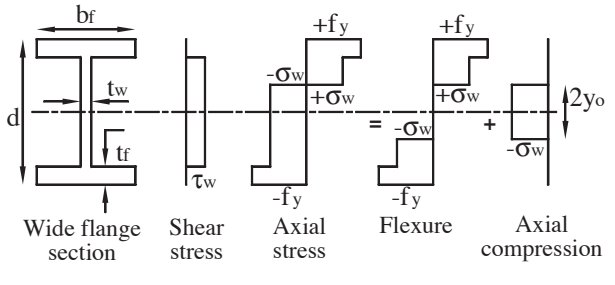

Fig. 3. Example of plastic resistance of a wide flange structural shape subjected to flexure, axial and shear forces.

Neglecting strain hardening, the plastic axial stress diagram of a typical wide flange section can be divided into pure flexural and axial contributions as shown in Figure 3. The contributions of the web and flanges to plastic moment can be calculated based on the flexural stress diagrams, respectively, as:

$$M_{pr-web}^{P,V} = \frac{t_w\left(d-2t_f\right)^2}{4}\sigma_w - \frac{t_w\left(2y_o\right)^2}{4}\sigma_w \tag{4}$$

$$M_{pr-flange}^{P,V} = b_f t_f \left(d-t_f\right) f_y \tag{5}$$

where the superscript (*P, V*) indicates that the plastic moment is reduced taking into account the applied axial and shear forces, and where b_f and t_f are the flange width and thickness of the cross section, respectively. Then, plastic moment of the cross section, $M_{pr}^{P,V}$, can be obtained as:

$$M_{pr}^{P,V} = M_{pr-web}^{P,V} + M_{pr-flange}^{P,V} \tag{6}$$

The preceding lower-bound approach, which provides acceptable results, has been used for steel moment frame design. However, for SPSWs, experimental results described in Qu et al. (2008) provide evidence that a more sophisticated procedure is warranted for intermediate HBEs. To do so, a review of the von Mises criterion in the plane stress condition is necessary and presented in the following section.

REDUCED YIELD STRENGTH IN HBE WEB

To better understand the reduced axial yield strength in an HBE web due to the presence of shear and vertical stresses, two elements are arbitrarily selected from the axial tension and compression zones of a segment of intermediate HBE

web as shown in Figure 4. These elements are in plane stress condition.

The results of classic mechanics of materials show that the von Mises yield criterion in plane stress condition can be written as:

$$\left(\frac{\sigma_x}{f_y}\right)^2-\left(\frac{\sigma_x}{f_y}\right)\left(\frac{\sigma_y}{f_y}\right)+\left(\frac{\sigma_y}{f_y}\right)^2+3\left(\frac{\tau_{xy}}{f_y}\right)^2=1 \qquad (7)$$

Equation 7 can be reorganized as a quadratic equation in terms of σ_x/f_w and solved to give the reduced axial yield strengths for given values of the other two terms:

$$\left(\frac{\sigma_x}{f_y}\right)=\frac{1}{2}\left(\frac{\sigma_y}{f_y}\right)\pm\frac{1}{2}\sqrt{4-3\left(\frac{\sigma_y}{f_y}\right)^2-12\left(\frac{\tau_{xy}}{f_y}\right)^2} \qquad (8)$$

Note that the reduced tension and compression axial yield strength can be obtained by considering the plus (+) and minus (–) solutions to Equation 8, respectively.

In the absence of vertical stress (i.e., $\sigma_y = 0$), the compression and tension axial yield strengths predicted by Equation 8 are of the same magnitude, which is

$$\left(\frac{\sigma_x}{f_y}\right)=\pm\sqrt{1-3\left(\frac{\tau_{xy}}{f_y}\right)^2} \qquad (9)$$

Note that Equation 9 is equivalent to Equation 2, which is used for estimating the plastic moment of wide flange members in steel moment frames.

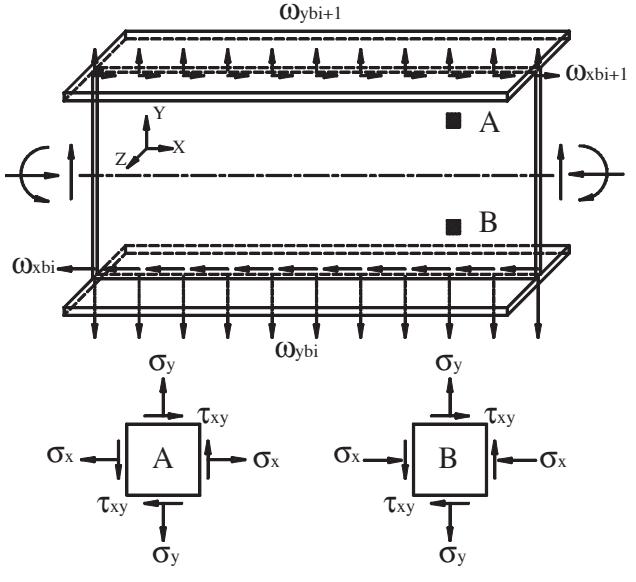

Fig. 4. Loading on the intermediate HBE segment.

The reduced tension and compression axial yield strengths, in the σ_x/f_y and σ_y/f_y space, for given values of τ_{xy}/f_y are shown in Figure 5, as a graphical representation of Equation 8. As shown, the tension and compression axial yield strengths are unequal due to the presence of vertical stresses. This is the stress condition found in the HBE web. Also note from Figure 5 that the compression axial yield strength is significantly reduced and can even become nil under the combined action of shear and vertical stresses. The tension axial yield strength is also affected by the shear and vertical stresses, but to a lesser degree. The maximum value of σ_y/f_y shown in Figure 5 is less than 1.0 in some cases (e.g., for the case of $\tau_{xy}/f_y = 0.40$) because the maximum allowable vertical stress (i.e., σ_y) is reduced due to the presences of axial and shear stresses (i.e., σ_x and τ_{xy}, respectively).

INTERMEDIATE HBE UNDER EQUAL TOP AND BOTTOM TENSION FIELDS

The plastic moment of an intermediate HBE under equal top and bottom tension fields is first discussed because this case provides some of the building blocks necessary to understand the more complex scenarios presented later.

Derivation of Plastic Moment

In the spirit of classic plastic cross-section analysis and using the reduced axial yield strength obtained from the von Mises yield criterion accounting for the vertical and shear stresses, one can generate the stress diagrams for a fully plastified HBE cross section under equal top and bottom tension fields. Note that all the equations derived in this section remain valid for cases of both flexures shown in Figure 6.

As traditionally done in structural steel for wide flange sections, uniform shear stress is assumed to act on the HBE web and is calculated according to Equation 1. In addition, a constant vertical tension stress is assumed in the HBE web as a result of the identical top and bottom tension fields, which is:

$$\sigma_y=\frac{\omega_{ybi}}{t_w} \qquad (10)$$

Consistent with Equation 8, the tension and compression axial yield strengths, σ_t and σ_c, can be calculated as:

$$\left(\frac{\sigma_t}{f_y}\right)=\frac{1}{2}\left(\frac{\sigma_y}{f_y}\right)+\frac{1}{2}\sqrt{4-3\left(\frac{\sigma_y}{f_y}\right)^2-12\left(\frac{\tau_w}{f_y}\right)^2} \qquad (11)$$

$$\left(\frac{\sigma_c}{f_y}\right)=\frac{1}{2}\left(\frac{\sigma_y}{f_y}\right)-\frac{1}{2}\sqrt{4-3\left(\frac{\sigma_y}{f_y}\right)^2-12\left(\frac{\tau_w}{f_y}\right)^2} \qquad (12)$$

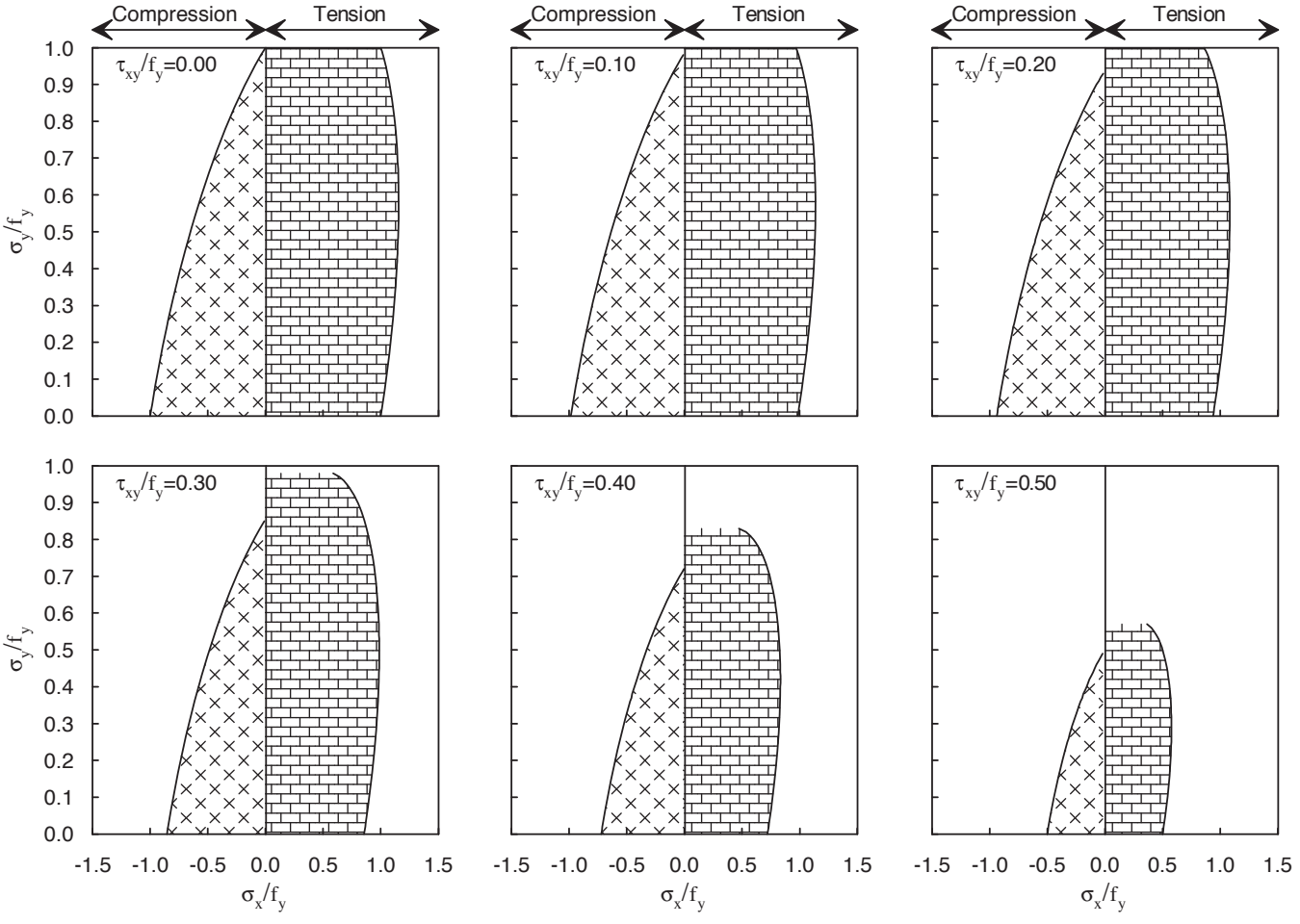

Fig. 5. Reduced yield strength per the von Mises yield criterion in plane stress.

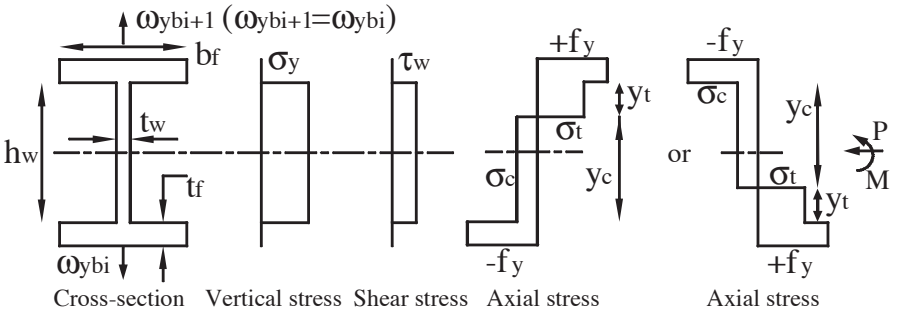

Fig. 6. Stress diagrams of intermediate HBE cross section under flexure, axial compression, shear force and vertical stresses due to equal top and bottom tension fields.

From the geometry in Figure 6,

$$y_t = h_w - y_c \tag{13}$$

where y_c and y_t represent compression and tension portion of the web, respectively.

For the common case that the neutral axis remains in the web, the governing equation of axial force equilibrium can be given as:

$$\sigma_c y_c t_w + \sigma_t y_t t_w = P \tag{14}$$

Note that the contribution of the flanges to axial compression is nil because the resultant axial force of each flange has the same magnitude but opposite sign (and thus each cancels the other).

Substituting Equation 13 into Equation 14 and solving for y_c gives

$$y_c = \frac{\left(\frac{\sigma_t}{f_y}\right) + \beta_w}{\left(\frac{\sigma_t}{f_y}\right) - \left(\frac{\sigma_c}{f_y}\right)} \times h_w \tag{15}$$

where β_w is the ratio of the applied axial compression to the nominal axial strength of the web, which is given by:

$$\beta_w = \frac{-P}{f_y h_w t_w} \tag{16}$$

The contributions of the web and flanges to the plastic moment of the whole cross section, M_{pr-web} and $M_{pr-flange}$, can be respectively determined as:

$$M_{pr-web} = \sigma_t t_w y_t \left(\frac{h_w}{2} - \frac{y_t}{2}\right) - \sigma_c t_w y_c \left(\frac{h_w}{2} - \frac{y_c}{2}\right) \tag{17}$$

$$M_{pr-flange} = f_y b_f t_f \left(d - t_f\right) \tag{18}$$

A cross-section plastic moment reduction factor, β, is defined to quantify the loss in plastic strength attributable to the combined effect of the axial compression, shear force and vertical stresses acting on the HBE web. The magnitude of β can be determined as:

$$\beta = \frac{M_{pr-web} + M_{pr-flange}}{f_y Z} \tag{19}$$

where Z is the plastic section modulus of HBE.

As shown in Equations 11 and 12, the acting direction of shear stresses (i.e., the sign of τ_w) has no impact on the resulting compression and tension axial yield strengths and, consequently, makes no difference in the calculated plastic moment reduction factor.

For the extreme case for which the HBE web makes no contribution to the flexural resistance, the minimum value of the reduction factor, β_{min}, is obtained and is given as:

$$\beta_{min} = \frac{M_{pr-flange}}{f_y Z} \tag{20}$$

This will happen when the entire web is under uniform compression.

Finite Element Verification

To validate the approach developed earlier to calculate the plastic moment reduction factor of intermediate HBEs under equal top and bottom tension fields, a series of finite element analyses was performed on a segment of HBE. The finite element model is shown in Figure 7.

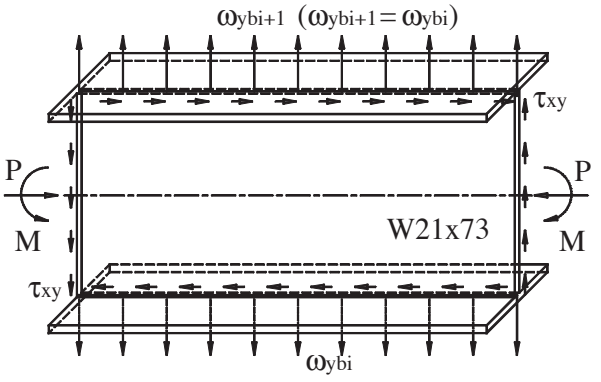

(*a*)

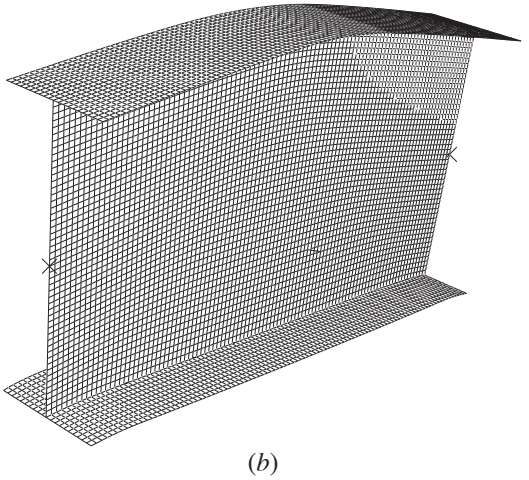

(*b*)

Fig. 7. Finite element model of intermediate HBE segment under flexure, axial compression, shear force and vertical stresses due to equal top and bottom tension fields.

In this case, a W21×73 member was modeled in ABAQUS/Standard (ABAQUS 2005). The length of this member was twice the cross-section depth. Material was assumed to be A572 Grade 50 steel with isotropic, elastic-perfectly-plastic constitutive behavior. A shell element (ABAQUS element S4R) was employed for the web and flanges. A fine mesh with 9,000 elements (2,000 elements per flange and 5,000 elements for the web) was used in this model.

As shown in Figure 7, uniform loads, ω_{ybi+1} and ω_{ybi}, of identical magnitude, but in opposite directions at the top and bottom edges of the HBE web, represented the vertical components of the top and bottom tension fields. Uniform shear stresses, τ_{xy}, were applied along the edges of the HBE web. Axial forces applied at the ends of the member represented the axial compression in the HBE.

The finite element analysis was conducted in two stages to correctly replicate the boundary conditions and to achieve the desired load scenario while keeping the whole model in self-equilibrium. In the first stage, the aforementioned tension fields, shear stresses and axial forces were applied on the model. In the second stage, a displacement-controlled analysis procedure was used in which the rotations of

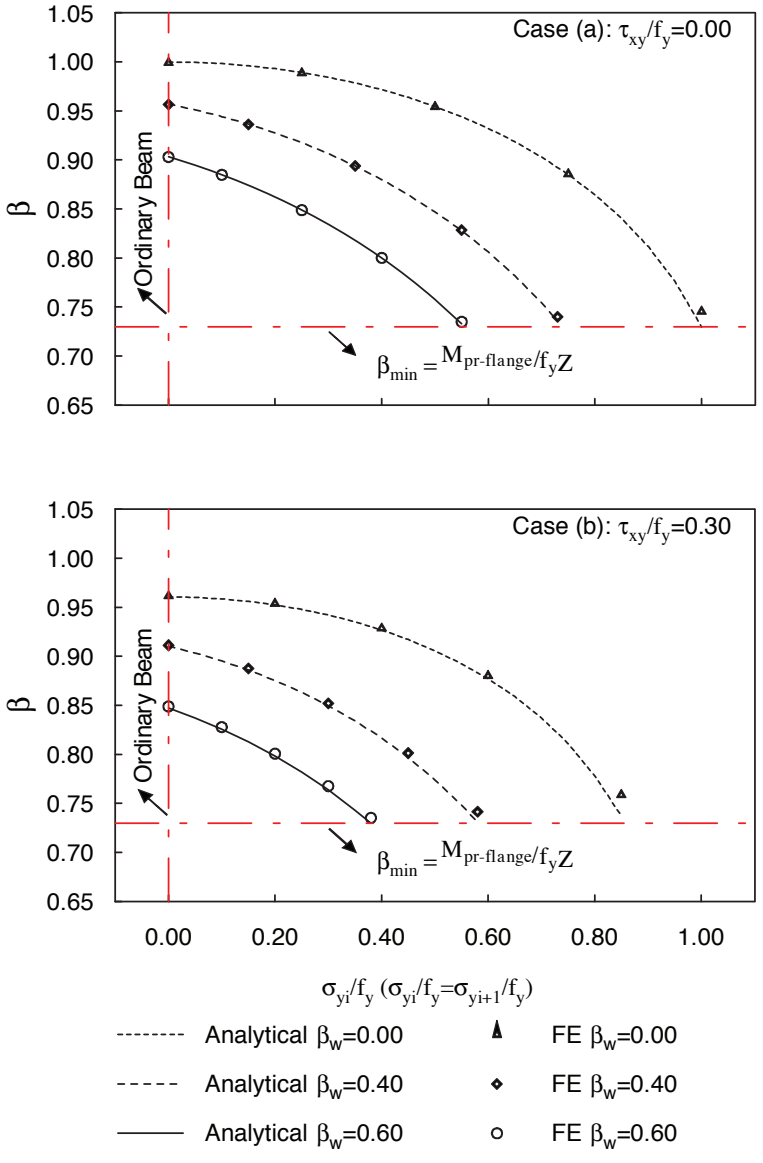

Fig. 8. Plastic moment reduction factor of intermediate HBE under axial compression, shear force and constant vertical stresses: analytical prediction versus finite element results.

opposite directions were proportionally increased up to a magnitude of 0.035 rad at the ends of the HBE segment to obtain the plastic moment strength A series of analyses was conducted on the finite element model to assess the accuracy of the analytical procedure. A comparison of results is given in Figure 8, which shows that the finite element analysis agrees with the analytical procedure. For the given axial compression and shear stresses, the magnitudes of the identical tension fields were increased from nil to the maximum value allowable in the HBE web to capture the entire range of solutions. For each case of β_w, five different vertical stress conditions (approximately equally spaced in the range of σ_y/f_y) were considered in the finite element models. Note that the axial compression, shear stresses and vertical stresses developed in the HBEs depend on the infill panel tension field actions and size and material property of the HBEs. As a result, the combined axial compression, shear stresses and vertical stresses selected for these analyses may not necessarily develop in a specific intermediate HBE. Also note that the plastic moment reduction factor of intermediate HBE shown in Figure 8 reduces to that which corresponds to the values of an ordinary beam in the absence of tension fields. As shown, the cross-section plastic moment reduction factor varies from unity to the minimum when increasing the shear stresses, axial forces and vertical stresses.

INTERMEDIATE HBE UNDER UNEQUAL TOP AND BOTTOM TENSION FIELDS

In many cases, the infill panels above and below intermediate HBE are of different thicknesses, which may result in unequal top and bottom tension fields when the expected plastic mechanism of the wall develops. This section investigates how the HBE plastic moment would be affected by the unequal top and bottom tension fields. As listed in Table 1, both the positive and negative flexures will be considered. The fundamental concepts and modeling assumptions previously presented still apply, except that a linear variation of vertical stresses is assumed instead of the prior constant vertical stresses.

Derivation of Plastic Moment under Positive Flexure

As shown in Figure 9, one can generate the stress diagrams for a fully plastified HBE cross section of elasto-perfectly plastic steel subjected to axial compression, shear, vertical stresses due to unequal top and bottom tension fields and positive flexure. As an approximation, linearly varying vertical stresses are assumed to act on the HBE web. Mathematically, this assumption is expressed as:

$$\frac{\sigma_y(y)}{f_y} = \left(\frac{\sigma_{yi}}{f_y}\right)\left(1 - \frac{y}{h_w}\right) + \left(\frac{\sigma_{yi+1}}{f_y}\right)\left(\frac{y}{h_w}\right) \tag{21}$$

where the vertical stresses at the top and bottom edges of the HBE web, σ_{yi+1} and σ_{yi}, can be calculated respectively as:

$$\sigma_{yi+1} = \frac{\omega_{ybi+1}}{t_w} \tag{22}$$

$$\sigma_{yi} = \frac{\omega_{ybi}}{t_w} \tag{23}$$

In accordance with Equation 8, the tension and compression axial yield strengths in the web can be respectively determined as:

$$\frac{\sigma_t(y)}{f_y} = \frac{1}{2}\frac{\sigma_y(y)}{f_y} + \frac{1}{2}\sqrt{4 - 3\left[\frac{\sigma_y(y)}{f_y}\right]^2 - 12\left(\frac{\tau_w}{f_y}\right)^2} \tag{24}$$

$$\frac{\sigma_c(y)}{f_y} = \frac{1}{2}\frac{\sigma_y(y)}{f_y} - \frac{1}{2}\sqrt{4 - 3\left[\frac{\sigma_y(y)}{f_y}\right]^2 - 12\left(\frac{\tau_w}{f_y}\right)^2} \tag{25}$$

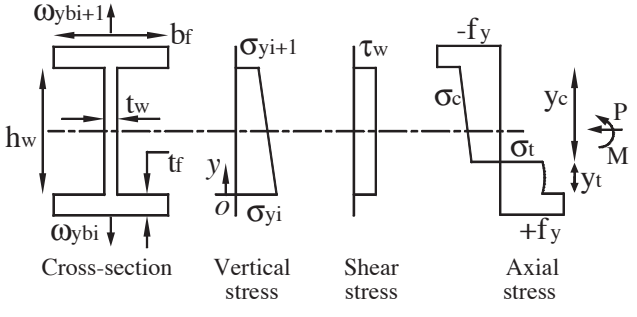

Fig. 9. Stress diagrams of intermediate HBE cross section under positive flexure, axial compression, shear force and vertical stresses due to unequal top and bottom tension fields.

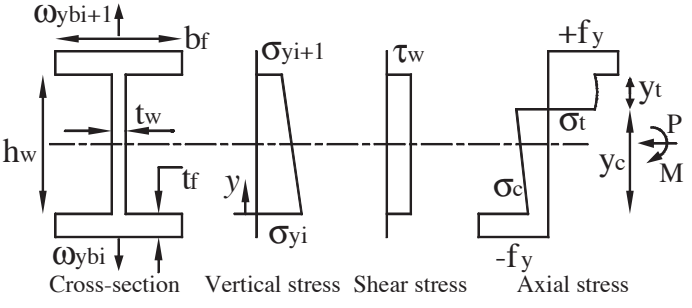

Fig. 10. Stress diagrams of intermediate HBE cross section under negative flexure, axial compression, shear force and vertical stresses due to unequal top and bottom tension fields.

Corresponding to Equation 14, the governing equation of axial force equilibrium can be given as:

$$\int_0^{h_w-y_c} \sigma_t(y)\,t_w\,dy + \int_{h_w-y_c}^{h_w} \sigma_c(y)\,t_w\,dy = P \tag{26}$$

Substituting Equations 24 and 25 into Equation 26, and also using the assumption expressed in Equation 21, gives the following equation:

$$\int_0^{h_w-y_c} \left\{ \begin{array}{l} \frac{1}{2}\left[\left(\frac{\sigma_{yi}}{f_y}\right)\left(1-\frac{y}{h_w}\right)+\left(\frac{\sigma_{yi+1}}{f_y}\right)\left(\frac{y}{h_w}\right)\right] \\ +\frac{1}{2}\sqrt{4-3\left[\left(\frac{\sigma_{yi}}{f_y}\right)\left(1-\frac{y}{h_w}\right)+\left(\frac{\sigma_{yi+1}}{f_y}\right)\left(\frac{y}{h_w}\right)\right]^2-12\left(\frac{\tau_{xy}}{f_y}\right)^2} \end{array} \right\} t_w\,dy$$
$$+\int_{h_w-y_c}^{h_w} \left\{ \begin{array}{l} \frac{1}{2}\left[\left(\frac{\sigma_{yi}}{f_y}\right)\left(1-\frac{y}{h_w}\right)+\left(\frac{\sigma_{yi+1}}{f_y}\right)\left(\frac{y}{h_w}\right)\right] \\ -\frac{1}{2}\sqrt{4-3\left[\left(\frac{\sigma_{yi}}{f_y}\right)\left(1-\frac{y}{h_w}\right)+\left(\frac{\sigma_{yi+1}}{f_y}\right)\left(\frac{y}{h_w}\right)\right]^2-12\left(\frac{\tau_{xy}}{f_y}\right)^2} \end{array} \right\} t_w\,dy = P \tag{27}$$

It is not possible to solve for the closed-form solution of y_c from Equation 27, but one may use software packages such as Mathcad to obtain the numerical solution of y_c. Then, knowing y_c, the contribution of the web to the plastic moment of the whole cross section can be determined as:

$$M_{pr-web} = \int_0^{h_w-y_c} \sigma_t(y)\left(\frac{h_w}{2}-y\right)t_w dy + \int_{h_w-y_c}^{h_w} \sigma_c(y)\left(\frac{h_w}{2}-y\right)t_w dy \tag{28}$$

For the contribution of the flanges, $M_{pr-flange}$, and the plastic moment reduction factor, β, Equations. 18 and 19 still apply.

Derivation of Plastic Moment under Negative Flexure

Results can also be generated following the same procedure for the case of negative flexure. The resulting stress diagrams are shown in Figure 10. All the equations developed to locate the neutral axis for the case of positive flexure remain valid, except that the integral limits of Equation 26 need to be modified as follows according to the stress diagrams shown in Figure 10:

$$\int_{y_c}^{h_w} \sigma_t(y)\,t_w\,dy + \int_0^{y_c} \sigma_c(y)\,t_w\,dy = P \tag{29}$$

Solving for y_c from Equation 29, one can obtain the contribution of the web to the plastic moment of the whole cross section as:

$$M_{pr-web} = \int_{y_c}^{h_w} \sigma_t(y)\left(y-\frac{h_w}{2}\right)t_w dy + \int_0^{y_c} \sigma_c(y)\left(y-\frac{h_w}{2}\right)t_w dy \tag{30}$$

For the contribution of the flanges to the moment resistance, $M_{pr-flange}$, and cross-section plastic moment reduction factor, β, Equations 18 and 19 remain valid.

Finite Element Verification

To validate the approach developed earlier for determining the plastic moment of intermediate HBEs under unequal top and bottom tension fields, a series of finite element analyses were performed. The finite element models for positive and negative flexure cases are shown in Figure 11.

The material, element, mesh, boundary condition and loading sequence are the same as those for intermediate HBEs under equal top and bottom tension fields, except that a surface traction was applied on the HBE web to achieve the transition between the unbalanced tension fields and satisfy vertical force equilibrium. The surface traction, *S*, can

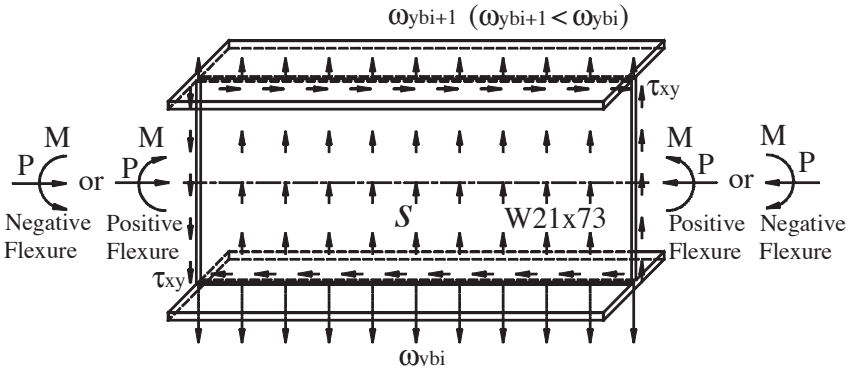

Fig. 11. Finite element model of intermediate HBE under flexure, axial compression, shear force and vertical stresses due to unequal top and bottom tension fields.

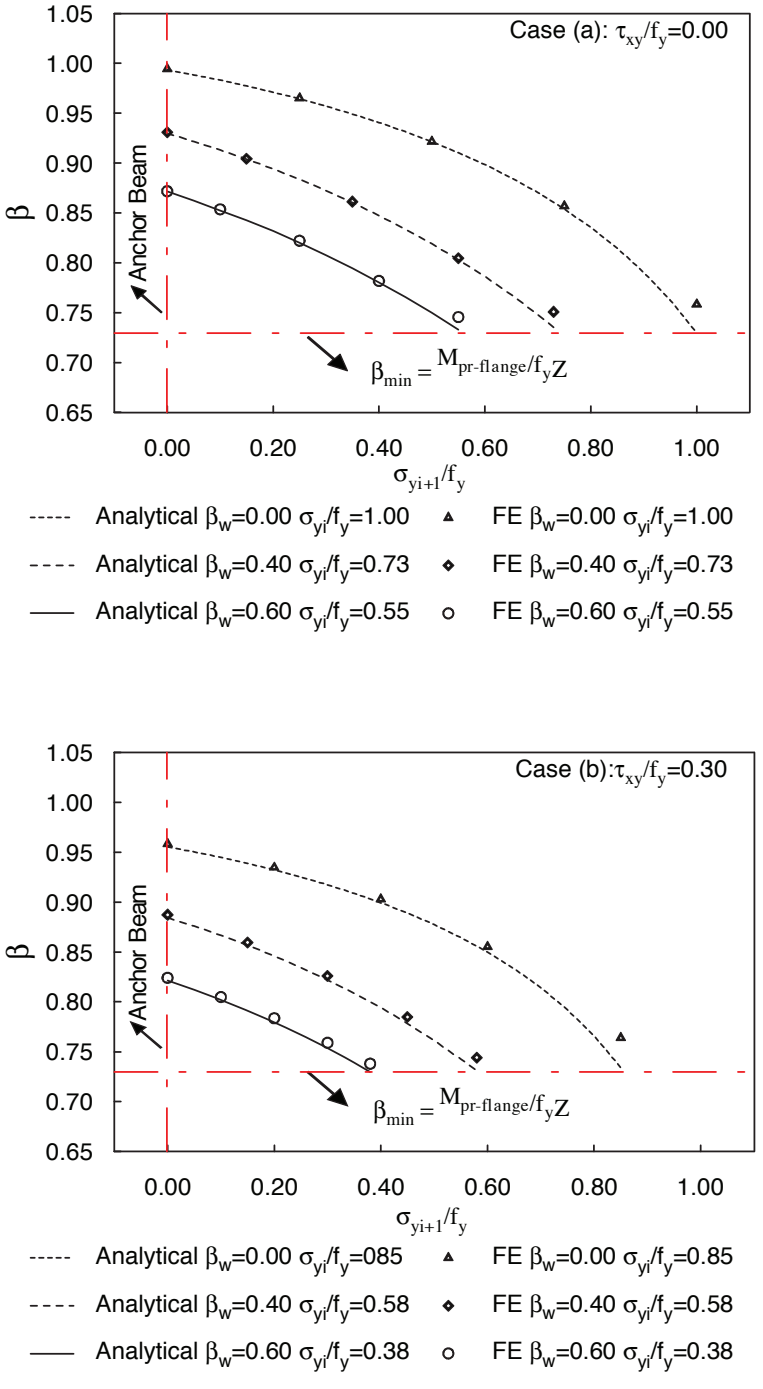

Fig. 12. Plastic moment reduction factor of intermediate HBE under positive flexure, axial compression, shear force and linear vertical stresses: analytical prediction versus finite element results.

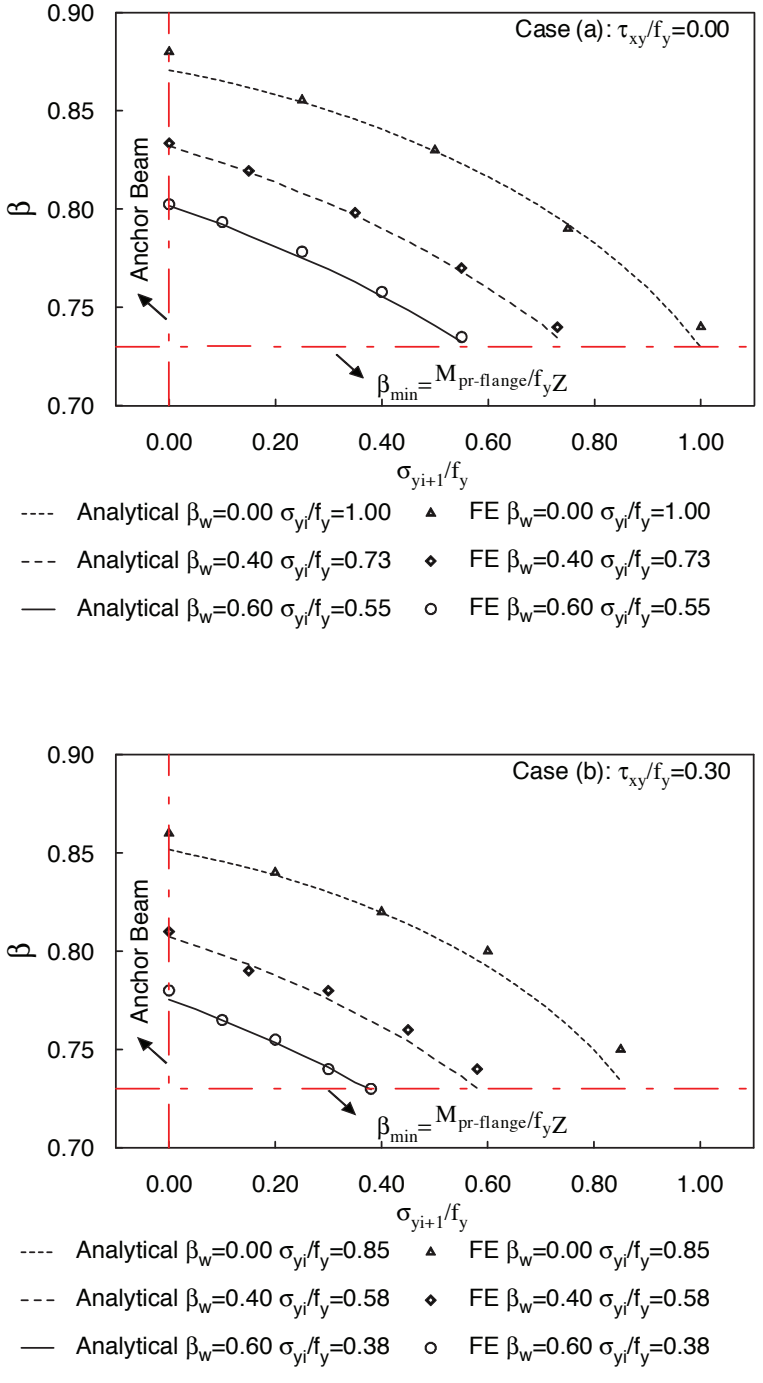

Fig. 13. Plastic moment reduction factor of intermediate HBE under negative flexure, axial compression, shear force and linear vertical stresses: analytical prediction versus finite element results.

be calculated as:

$$S = \frac{\omega_{ybi} - \omega_{ybi+1}}{h_w} \tag{31}$$

Note that, in reality, no such traction force is applied on the HBE web, because the unbalanced infill panel yield forces are equilibrated similarly to a uniformly distributed load on a beam. However, in modeling only a small beam segment as done earlier, the application of *S* keeps the segment in self-equilibrium and guarantees linear distribution of vertical stresses in the HBE web, consistent with the assumption used for derivation of the analytical procedures.

A series of analyses was conducted using the finite element models described earlier to assess the accuracy of the analytical procedures. In these analyses, for the given axial compression and shear force, the vertical component of the bottom tension field was kept constant and various magnitudes of the vertical component of the top tension field were considered—from zero up to a value equal to that of the bottom tension field. This range of infill panel yield forces acting on the top tension field starts from an intermediate HBE cross-section equivalent to an anchor HBE cross section in the absence of the top tension field and ends with the previously considered case of an intermediate HBE cross section under equal top and bottom tension fields.

Comparisons of the results from finite element analysis with those obtained following the analytical procedures are shown in Figures 12 and 13 for the positive and negative flexure cases, respectively. It is shown that the plastic moment of intermediate HBE under unequal top and bottom tension fields can be accurately estimated using the analytical procedures. The plastic moment reduction factor varies from unity to the minimum determined by Equation 20 as a result of the increasing shear force, axial force and vertical stresses.

Comparing the results shown in Figure 12 with those shown in Figure 13, it is also possible to observe that for the same combination of axial compression, shear forces and vertical stresses, the plastic moment under positive flexure is greater than that under negative flexure. For example, according to case a shown in Figure 12, the plastic moment reduction factor is 0.97 for an intermediate HBE under positive flexure for which $\tau_{xy}/f_y = 0.00$, $\beta_w = 0.00$, $\sigma_{yi}/f_y = 1.00$, and $\sigma_{yi+1}/f_y = 0.20$; however, a smaller value of 0.86 is obtained for the corresponding negative flexure case as shown in case a of Figure 13. This can be explained on the basis that higher vertical stresses are acting at the bottom of the beam segment, which is also in axial compression in the negative flexure case. Recall from Figure 5 (which shows yielding under biaxial loading conditions, per the von Mises yield criterion) that the compression axial yield strength is more reduced by the presence of vertical stresses than the tension axial yield strength. Therefore, the plastic moment is reduced more in the negative flexure case than the positive flexure case.

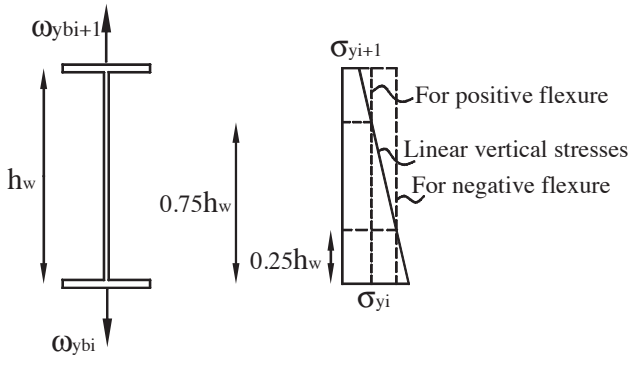

Fig. 14. Simplification of vertical stress distribution.

Simplification of Analytical Procedures

Although the analytical procedures to estimate the plastic moment of intermediate HBE under unequal top and bottom tension fields were developed and verified by finite element results, impediments exist that may limit the acceptance of this approach in design practice. For example, there are challenges in solving for y_c from Equations 27 and 29 using simple calculations. The mathematical difficulty results from the presence of nonconstant vertical stresses.

Aiming at the kind of simple equations derived to calculate the plastic moment of intermediate HBE under equal top and bottom tension fields, for which constant vertical stress is assumed, it would be expedient to replace the linearly varying vertical stresses in the case at hand by an equivalent constant vertical stress. However, it would not be appropriate to use a constant vertical stress of magnitude equal to the average stress of the linearly varying vertical stresses as an approximation, because such a unique equivalent constant vertical stress would result in identical plastic moments for both positive and negative flexure cases. This is inconsistent with the prior observations from Figures 12 and 13.

As a compromise between simplicity and accuracy, to consider the different effects of vertical stresses on plastic moment of intermediate HBEs under positive and negative flexures, the magnitudes of those stresses at the three-fourths and one-fourth points of the linearly varying stress diagram, as shown in Figure 14, are taken as the magnitudes of the equivalent constant vertical stresses for the positive and negative flexure cases, respectively. Mathematically, the magnitudes of these equivalent constant vertical stress distributions can be expressed as:

$$\sigma_{y-uni} = \frac{1}{2}\left(\sigma_{yi} + \sigma_{yi+1}\right) \pm \frac{1}{4}\left(\sigma_{yi} - \sigma_{yi+1}\right) \tag{32}$$

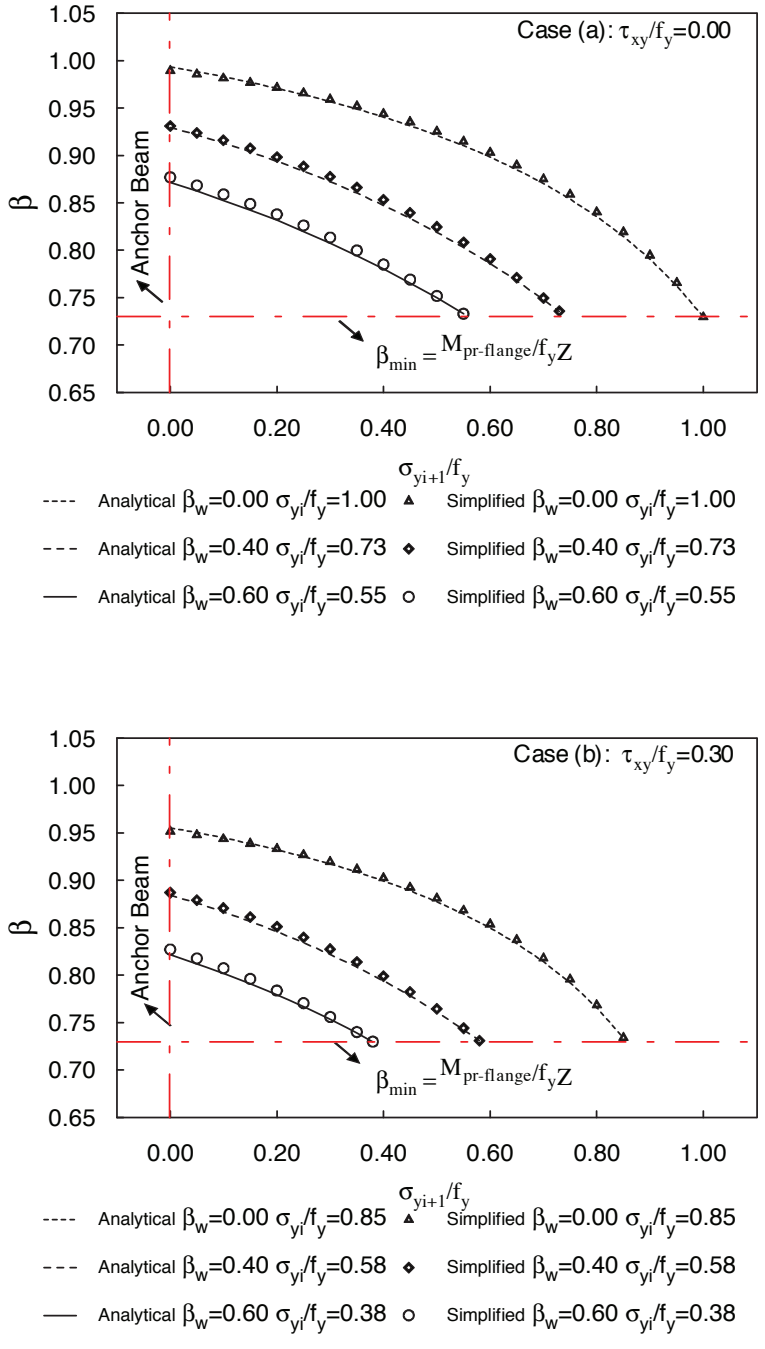

Fig. 15. Plastic moment reduction factor of intermediate HBE under positive flexure, axial compression, shear force and linear vertical stresses: analytical prediction versus simplified approach.

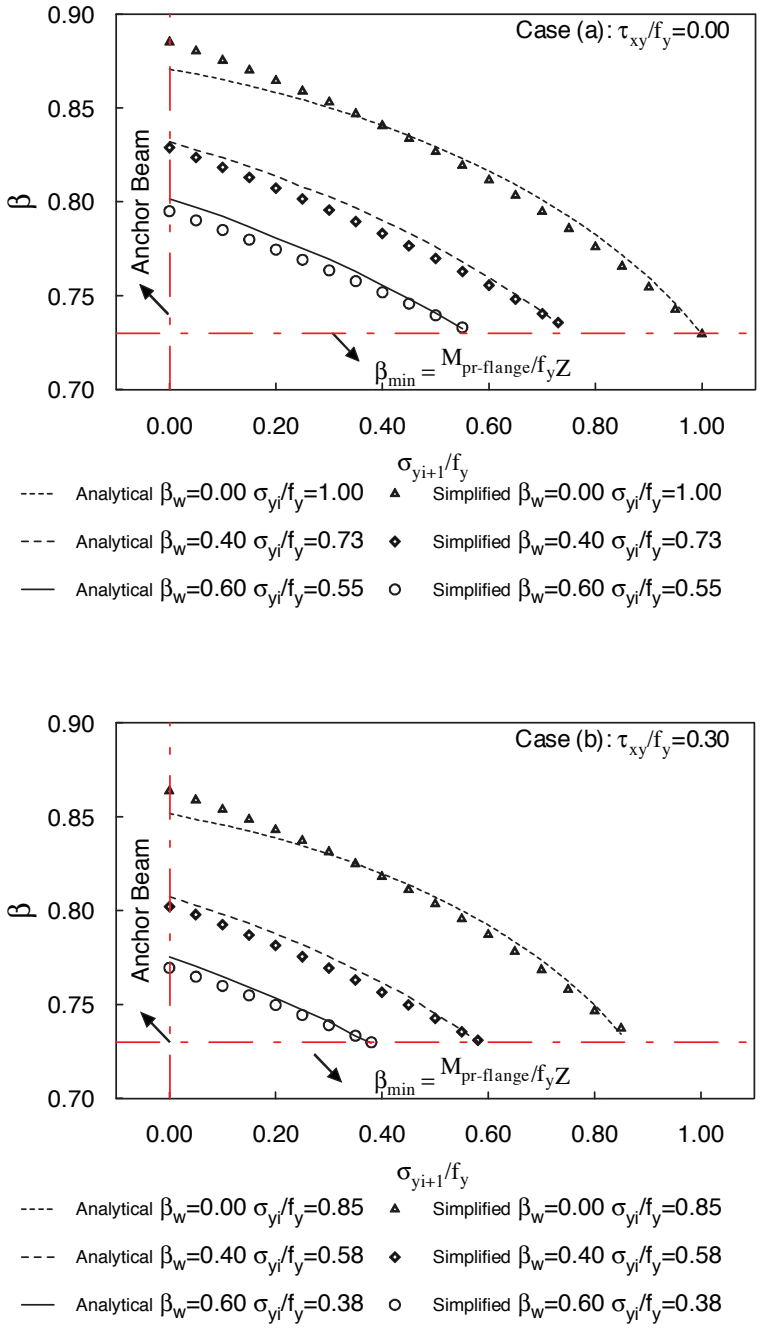

Fig. 16. Plastic moment reduction factor of intermediate HBE under negative flexure, axial compression, shear force and linear vertical stresses: analytical prediction versus simplified approach.

Minus (–) and plus (+) signs are employed in Equation 32 for the positive and negative flexure cases, respectively. Then, the procedures to determine the plastic moment of intermediate HBE under equal top and bottom tension fields can be used.

To check the adequacy of this model, the results obtained using the preceding simplified procedure are compared with those using the more rigorous analytical procedures developed earlier in Figures 15 and 16 for positive and negative flexure cases, respectively. It is found that the simplified procedure provides reasonable and relatively efficient estimates of the cross-section plastic moment reduction factors, although slightly less accurate results are observed in the negative flexure case.

ADDITIONAL DISSCUSSION ON ANCHOR HBE

Results developed for intermediate HBEs under unequal top and bottom tension fields can also be applied for anchor HBE because anchor HBE is only a special case of intermediate HBE for which the tension field is only applied on one side. This can be achieved by setting σ_{yi+1} equal to zero in all equations derived in previous section. Although examples shown in Figures 12, 13, 15 and 16 only provide results for anchor HBEs in limited scenarios (i.e., only loading scenarios corresponding to the left ends of those curves), additional examples developed by Qu and Bruneau (2008) further confirmed that the analytical procedures and simplified models for estimating the plastic moment of intermediate HBEs under unequal top and bottom tension fields remain valid for anchor HBEs.

CONCLUSIONS

Analytical procedures for estimating the plastic moments of intermediate HBEs of SPSWs have been developed in this paper. Those procedures are based on classic plastic analysis and rely on calculation of the reduced axial yield strength of HBE web accounting for the presence of shear and vertical stresses. Results from these procedures were shown to agree well with the results from finite element analysis. Simplified models developed for practical purposes were shown to be accurate. These formulations presented here were critical to explain the behavior observed experimentally in prior tests; see Qu and Bruneau (2010) for comparisons of test results with results from finite element analyses (similar to those for which the closed-form equations presented here have been shown to give satisfactory results). Implementation of the developed analytical procedure is necessary to achieve capacity design of HBE-to-VBE connections, which ensures desirable performance of HBEs.

ACKNOWLEDGMENTS

This work was supported by the Earthquake Engineering Research Centers Program of the National Science Foundation under award number ECC-9701471 to the Multidisciplinary Center for Earthquake Engineering Research. Any opinions, findings, conclusions and recommendations presented in this paper are those of the writers and do not necessarily reflect the views of the sponsors.

SYMBOLS

M = moment acting at HBE cross section

P = axial compression acting at HBE cross section

Z = plastic section modulus

b_f = flange width of the cross section

d = depth of the cross section

f_y = yield strength of steel

h_w = web depth of the cross section

t_f = flange thickness of the cross section

t_w = web thickness of the cross section

y_c = compression portion in the web of the cross section

y_t = tension portion in the web of the cross section

y_o = location of the neutral axis

σ_w = maximum axial stress that can be applied on the web of the cross section

σ_{yi} = vertical stress in HBE web

τ_w = shear stress acting on the web of the cross section

ω_{ybi} = vertical components of the infill panel forces

REFERENCES

ABAQUS (2005), *ABAQUS Analysis User's Manual* (version 6.5), Hibbitt, Karlsson, and Sorenson, Pawtucket, RI.

AISC (2010), ANSI/AISC 341-10, *Seismic Provisions for Structural Steel Buildings*, American Institute of Steel Construction, Chicago, IL.

Berman, J.W. and Bruneau, M. (2003a), "Experimental Investigation of Light-Gauge Steel Plate Shear Walls for the Seismic Retrofit of Buildings," *Technical Report MCEER-03-0001*, Multidisciplinary Center for Earthquake Engineering Research, Buffalo, NY.

Berman, J.W., and Bruneau, M. (2003b), "Plastic Analysis and Design of Steel Plate Shear Walls," *Journal of Structural Engineering*, Vol. 129, No. 11.

Bruneau, M., Uang, C.M. and Whittaker, A.S., (1998), *Ductile Design of Steel Structures,* McGraw-Hill Companies, Inc., New York, NY.

CSA (2009), CAN/CSA S16-01*, Limit States Design of Steel Structures,* Willowdale, ON, Canada.

Driver, R.G., Kulak, G.L., Kennedy, D.J.L. and Elwi, A.E. (1997), "Seismic Behavior of Steel Plate Shear Walls," *Structural Engineering Report No.215*, University of Alberta, Edmonton, AB, Canada.

Elgaaly, M., Caccese, V. and Du, C. (1993), "Postbuckling Behavior of Steel-Plate Shear Walls under Cyclic Loads," *Journal of Structural Engineering*, Vol. 119, No. 2.

Qu, B. and Bruneau, M. (2008), "Seismic Design of Boundary Frame Members of Steel Plate Shear Walls," *Technical Report MCEER-08-0012*, Multidisciplinary Center for Earthquake Engineering Research, Buffalo, NY.

Qu, B., Bruneau, M., Lin, C.H. and Tsai, K.C. (2008), "Testing of Full Scale Two-Story Steel Plate Shear Walls with RBS Connections and Composite Floor," *Journal of Structural Engineering*, Vol. 134, No. 3.

Qu, B. and Bruneau, M. (2010), "Capacity Design of Intermediate Horizontal Boundary Elements of Steel Plate Shear Walls," *Journal of Structural Engineering*, Vol. 135, No. 12.

Sabelli, R. and Bruneau, M. (2006), *Design Guide 20: Steel Plate Shear Walls,* American Institute of Steel Construction, Chicago, IL.

Thorburn, L.J., Kulak, G.L. and Montgomery, C.J. (1983), "Analysis of Steel Plate Shear Walls," *Structural Engineering Report No. 107*, Department of Civil Engineering, The University of Alberta, Edmonton, AB, Canada.

Tsai, K.C. and Lee, C.S. (2007), "Slender SPSW," *Technical Report NCREE-06-017*, National Center for Research on Earthquake Engineering. Taipei, Taiwan (in Chinese).

Vian, D. and Bruneau, M. (2005), "Steel Plate Shear Walls for Seismic Design and Retrofit of Building Structure," *Technical Report MCEER-05-0010*, Multidisciplinary Center for Earthquake Engineering Research, Buffalo, NY.